nature biomedical engineering

SUPPLEMENTARY INFORMATION

https://doi.org/10.1038/s41551-018-0261-7

In the format provided by the authors and unedited.

Tissue-adhesive wirelessly powered optoelectronic device for metronomic photodynamic cancer therapy

Kento Yamagishi[1], Izumi Kirino[2], Isao Takahashi[1], Hizuru Amano[3,4], Shinji Takeoka[1,5], Yuji Morimoto[6*] and Toshinori Fujie[7,8*]

[1]Graduate School of Advanced Science and Engineering, Waseda University, Tokyo, Japan. [2]Division of Hepato-Biliary-Pancreatic Surgery and Transplantation, Department of Surgery, Graduate School of Medicine, Kyoto University, Kyoto, Japan. [3]Institute of Advanced Active Aging Research, Waseda University, Tokyo, Japan. [4]Department of Pediatric Surgery, Graduate School of Medicine, The University of Tokyo, Tokyo, Japan. [5]Waseda Research Institute for Science and Engineering, Waseda University, Tokyo, Japan. [6]Department of Physiology, National Defense Medical College, Saitama, Japan. [7]Waseda Institute for Advanced Study, Waseda University, Tokyo, Japan. [8]Japan Science and Technology Agency, PRESTO, Saitama, Japan. *e-mail: moyan@ndmc.ac.jp; t.fujie@aoni.waseda.jp

Table of contents

Tables:

Figures:

Supplementary Fig. 13 | Temperature increase of implants.

Legends for Supplementary Videos 1-7.

Supplementary Table 1 | Mechanical properties of PDMS nanosheets. The centre values and measures of error represent the mean and the standard deviation (s.d.), respectively. n = 3 (different batches) for each sample.

Base : curing	Thickness (nm)	Elastic modulus (MPa)	Ultimate tensile strength (MPa)	Ultimate tensile elongation (%)
5 : 1	604 ± 43	4.36 ± 2.57	1.05 ± 0.07	39.1 ± 18.1
10 : 1	561 ± 87	1.47 ± 1.11	0.55 ± 0.12	70.8 ± 14.9
20 : 1	498 ± 13	0.41 ± 0.39	0.26 ± 0.01	41.3 ± 27.4

Supplementary Table 2 | Mechanical properties of pristine PDMS and PDA-PDMS nanosheets. The centre values and measures of error represent the mean and the s.d., respectively. n = 3 (different batches) for each sample.

Base:curing	PDA-modification	Thickness (nm)	Elastic modulus (MPa)	Ultimate tensile strength (MPa)	Ultimate tensile elongation (%)
10:1	Pristine	561 ± 87	1.47 ± 1.11	0.55 ± 0.12	70.8 ± 14.9
	24 h	654 ± 60	14.9 ± 0.60	1.72 ± 0.30	12.4 ± 7.0

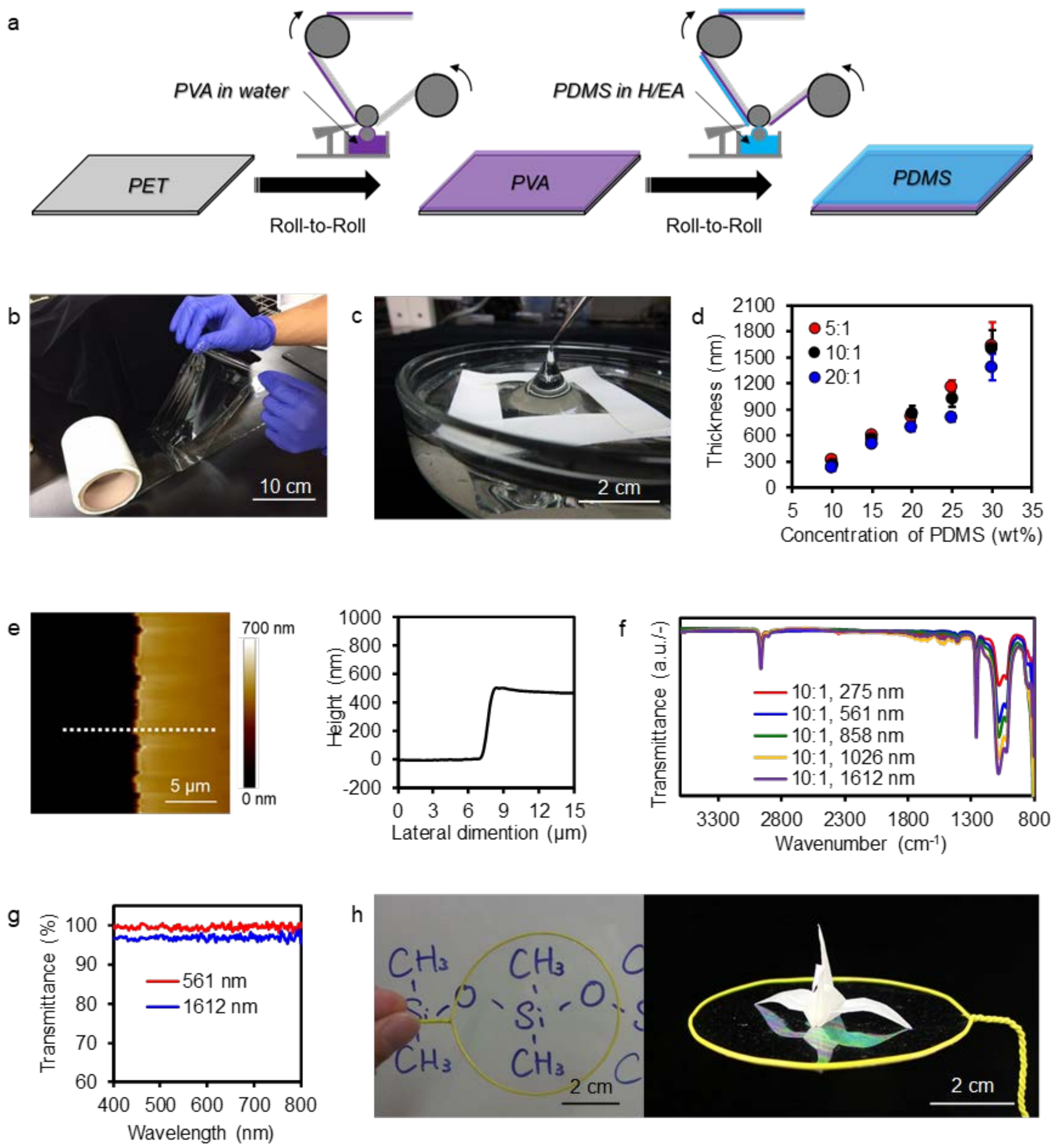

Supplementary Fig. 1 | Preparation and characterization of PDMS nanosheets. a, Schematic of preparation of PDMS/PVA bilayered film on a PET substrate by a roll-to-roll processed gravure coating. **b**, Image of PVA/PDMS bilayered film peeled off from a PET substrate. **c**, Image of a stretched PDMS nanosheet supported by an adhesive tape frame in water. **d**, Relationship between the concentration of PDMS in the solvent and the thickness of PDMS nanosheets with three different base polymer/curing agent ratios. The error bars and the measures of centre represent the s.d. and the mean, respectively (n

= 3 different batches for each sample). **e**, AFM height image (left) of the edge of the transferred PDMS nanosheet on a SiO_2 substrate and its cross-sectional profile (right). The observation was repeated for three different samples and a similar image and cross-sectional profile were obtained for every experiment. The representative data are shown. **f**, IR spectra of PDMS nanosheets with different thicknesses (base/curing agent ratio: 10/1). **g**, Transmittance spectra of PDMS nanosheets (thickness: 561 and 1612 nm) in the range of visible light (wavelength: 400-800 nm). **h**, Images of PDMS nanosheet (561 nm) supported by a wire-loop to show the transparency and robustness. Left: A chemical structure of PDMS drawn on a white board was visible through the PDMS nanosheet. Right: A paper crane (ca. 1.2 g) sustained on the PDMS nanosheet.

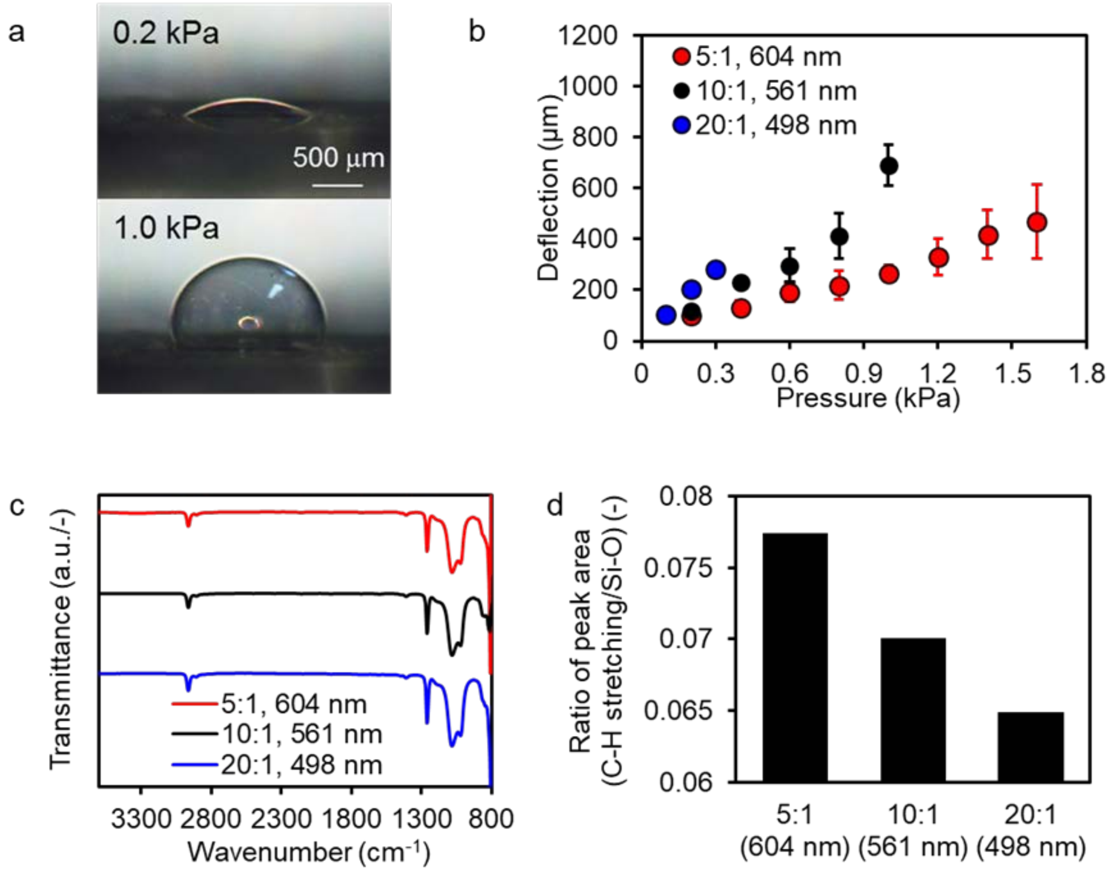

Supplementary Fig. 2 | Characterization of PDMS nanosheets with different base/curing agent ratios. a, Sequential cross-sectional views of the deflections at pressures of 0.2 (top) and 1.0 kPa (bottom) of the PDMS nanosheets (base/curing agent ratio: 10/1, 561 nm thick) during an air bulge test. The air bulge test was repeated for three different samples and a similar result was obtained for every experiment. The representative images are shown. **b**, Relationship between applied air pressure and deflection of the PDMS nanosheets. The error bars and the measures of centre represent the s.d. and the mean, respectively (n = 3 for each sample). **c**, IR spectra of PDMS nanosheets with different base/curing agent ratios. The FT-IR analysis was repeated for three different samples for each ratio and a similar result was obtained for every experiment. The representative spectra are shown. **d**, Ratios of C-H stretching/Si-O peak of PDMS nanosheets with different base/curing agent ratios.

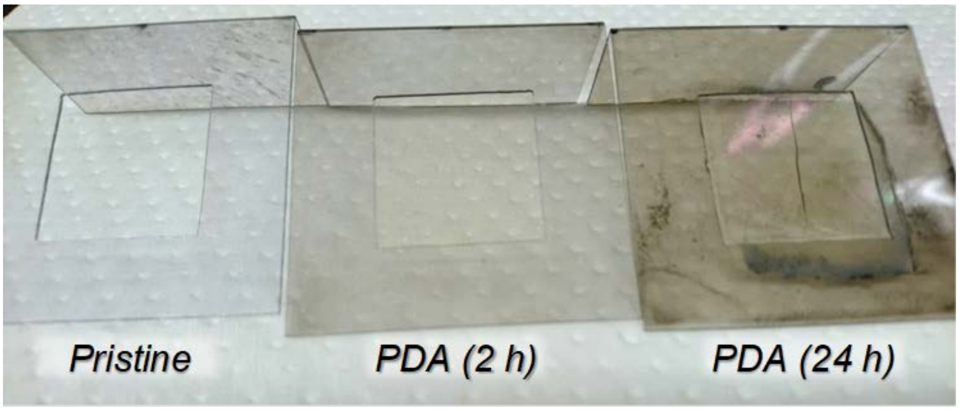

Supplementary Fig. 3 | Images of pristine and PDA-modified (2- and 24-h immersion in dopamine solution) PDMS nanosheets.

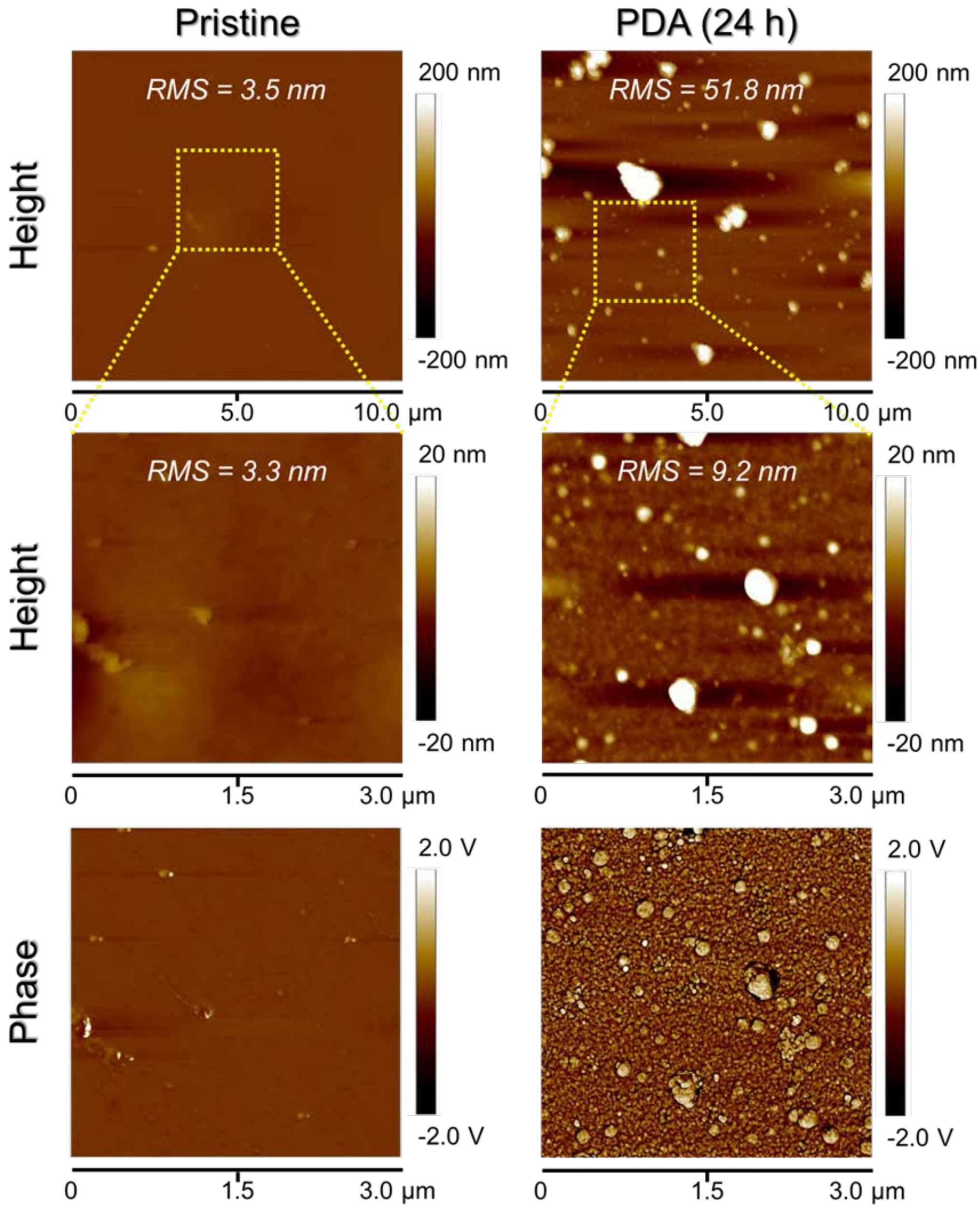

Supplementary Fig. 4 | AFM characterization of pristine PDMS and PDA-PDMS nanosheets. Height (top and middle) and phase (bottom) images of the pristine PDMS nanosheet (left, ca. 560 nm thick) and 24-h-modified PDA-PDMS nanosheet (right, ca. 650 nm thick). The AFM analysis was repeated for three different samples for both nanosheets and a similar image was obtained for every experiment. The representative images are shown.

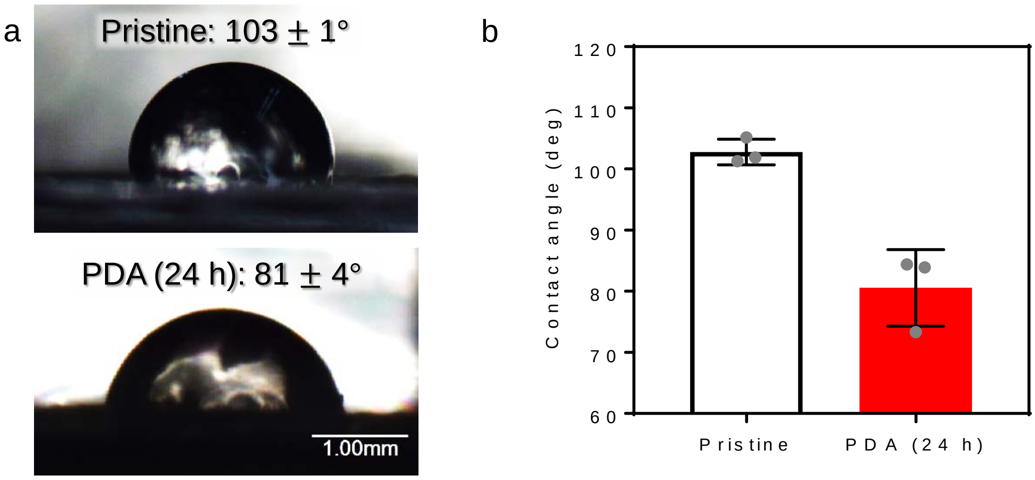

Supplementary Fig. 5 | Contact angle measurement. a, Images of contact angle measurement of a pristine PDMS nanosheet (top, 560 nm) and a 24-h-modified PDA-PDMS nanosheet (bottom, 650 nm). The contact angle measurement was repeated for three different samples for both nanosheets and a similar result was obtained for every experiment. The representative data are shown. **b**, Contact angles of the PDMS nanosheet and the PDA-PDMS nanosheet. The error bars and the measures of centre represent the s.d. and the mean, respectively (n = 3 for each sample). Each data point is overlaid on the bars as gray dot plots.

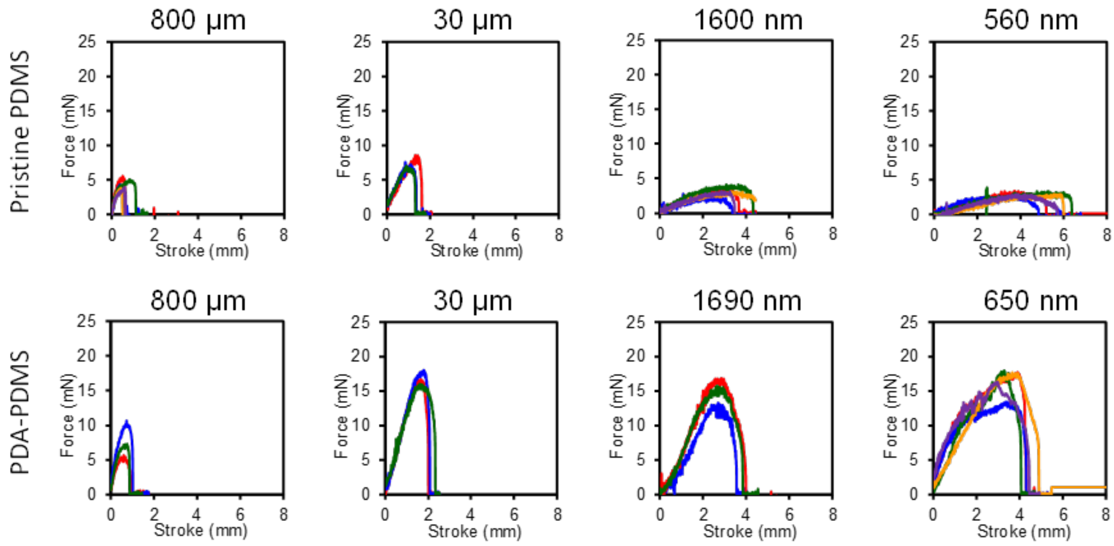

Supplementary Fig. 6 | Adhesiveness of PDMS films to chicken muscle. Tack separation force *vs*. separation stroke for pristine (top) and PDA-modified (bottom) PDMS films with different thicknesses adhered to chicken muscle. Three or five different samples were tested for each group and all of the results are shown.

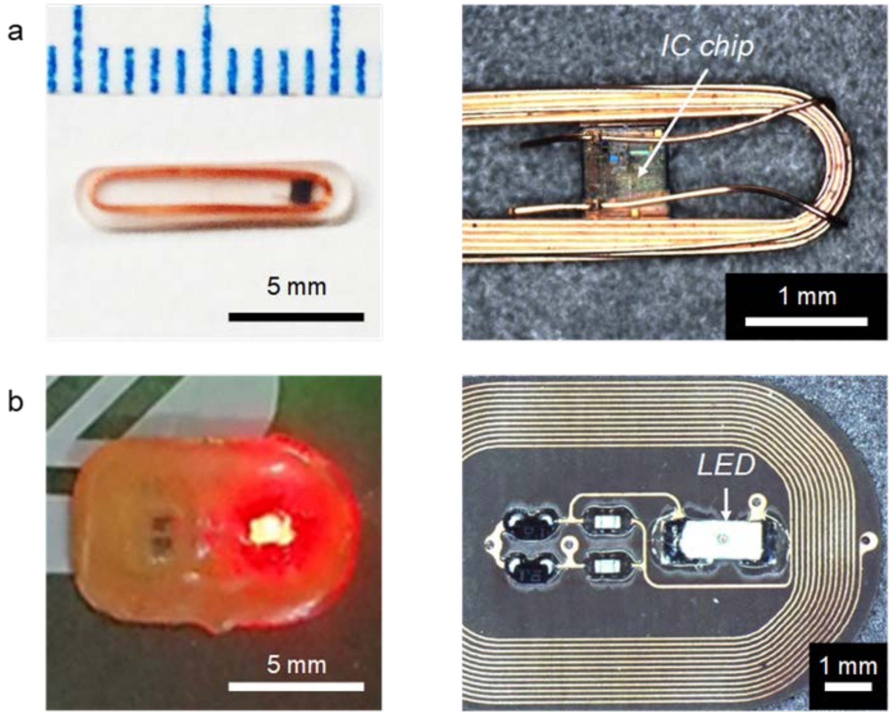

Supplementary Fig. 7 | Images of IC tag and LED chip. Digital (left) and microscopic (right) images of IC tag (**a**) and LED chip (**b**).

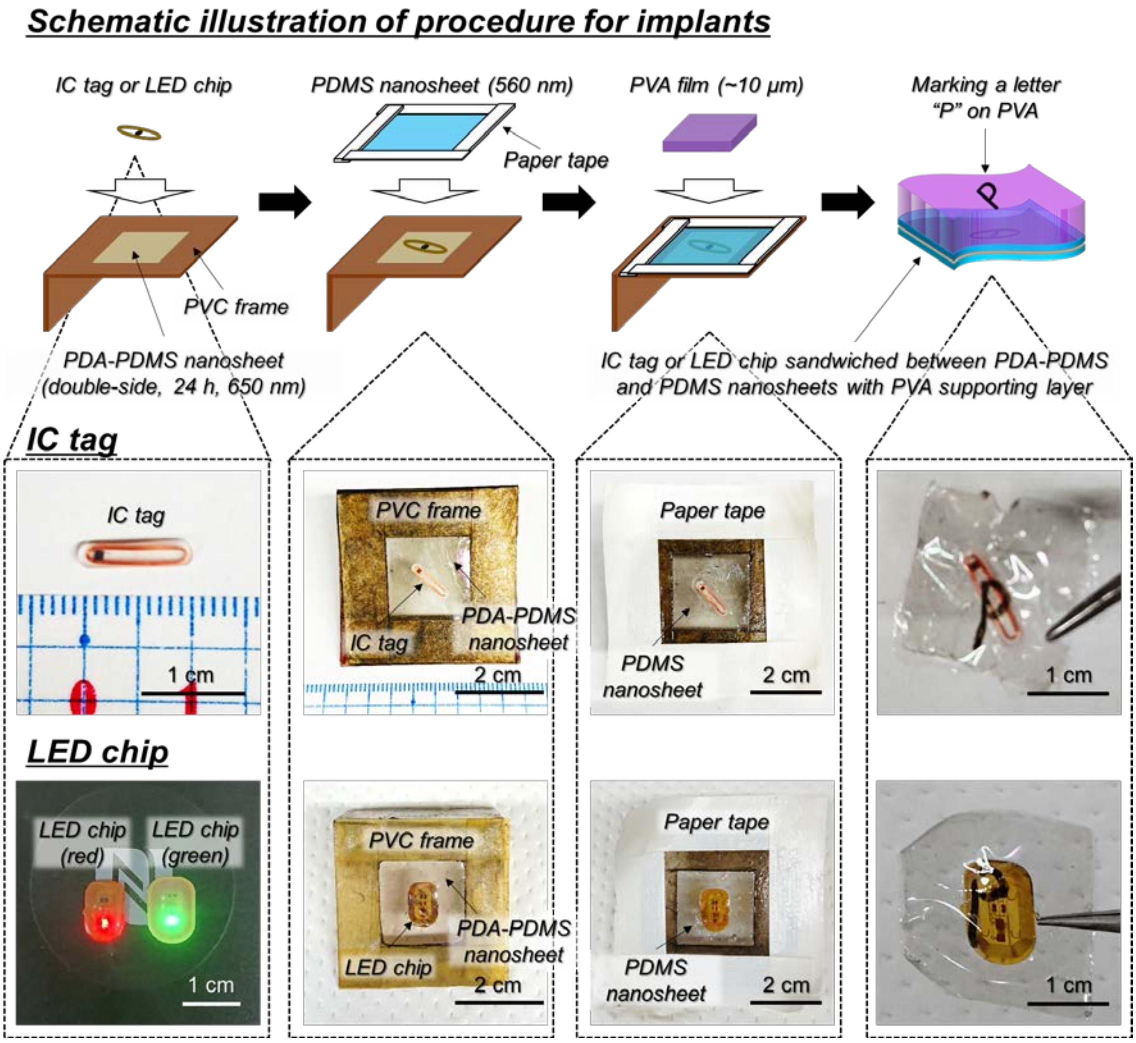

Supplementary Fig. 8 | Construction of the tissue-adhesive implants. Schematic illustration (top) and images (middle for IC tag and bottom for LED chip) for the construction of the tissue-adhesive implants. An IC tag or an LED chip was placed on a 24-h-double-side-modified PDA-PDMS nanosheet (650 nm thick) supported by a PVC frame. A pristine PDMS nanosheet (560 nm thick) supported by an adhesive tape frame was placed over the device to form a sandwich structure. A 10-μm-thick PVA film (2 × 2 cm) was attached to the pristine PDMS side as a water-soluble support layer. The implant with a layered structure (PDA-PDMS nanosheet/IC tag or LED chip/pristine PDMS nanosheet/PVA film) was cut off from the frame by cutting the border between the film and the frame with a knife.

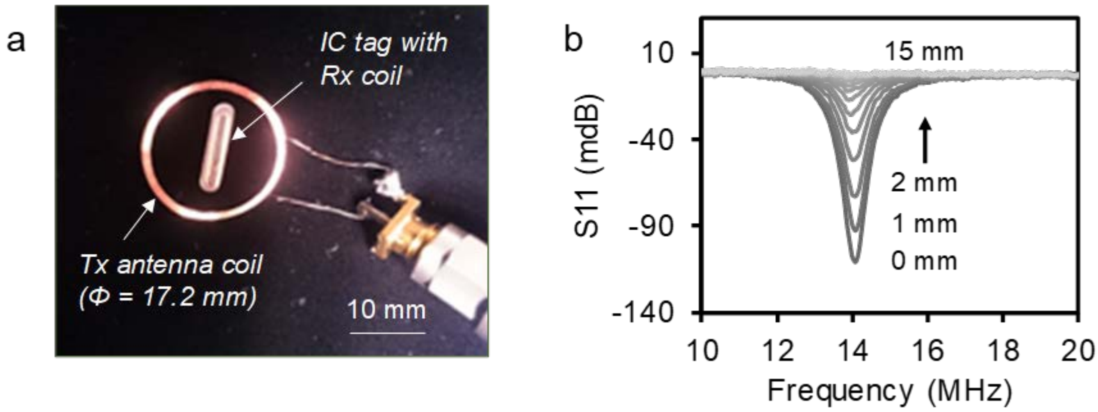

Supplementary Fig. 9 | Reflection scattering parameter (S11) measurement of IC tag. **a,** Image for the measurement of the resonant frequency of an IC tag with Rx coil by using an Tx antenna coil (diameter: 17.2 mm) connected to a network analyzer. **b,** S11 signal vs. frequency for different vertical distances (from 0 to 15 mm) between the IC tag and the Tx antenna coil in the air. The S11 measurement was repeated for three different IC tags and a similar result was obtained for every experiment. The representative data are shown.

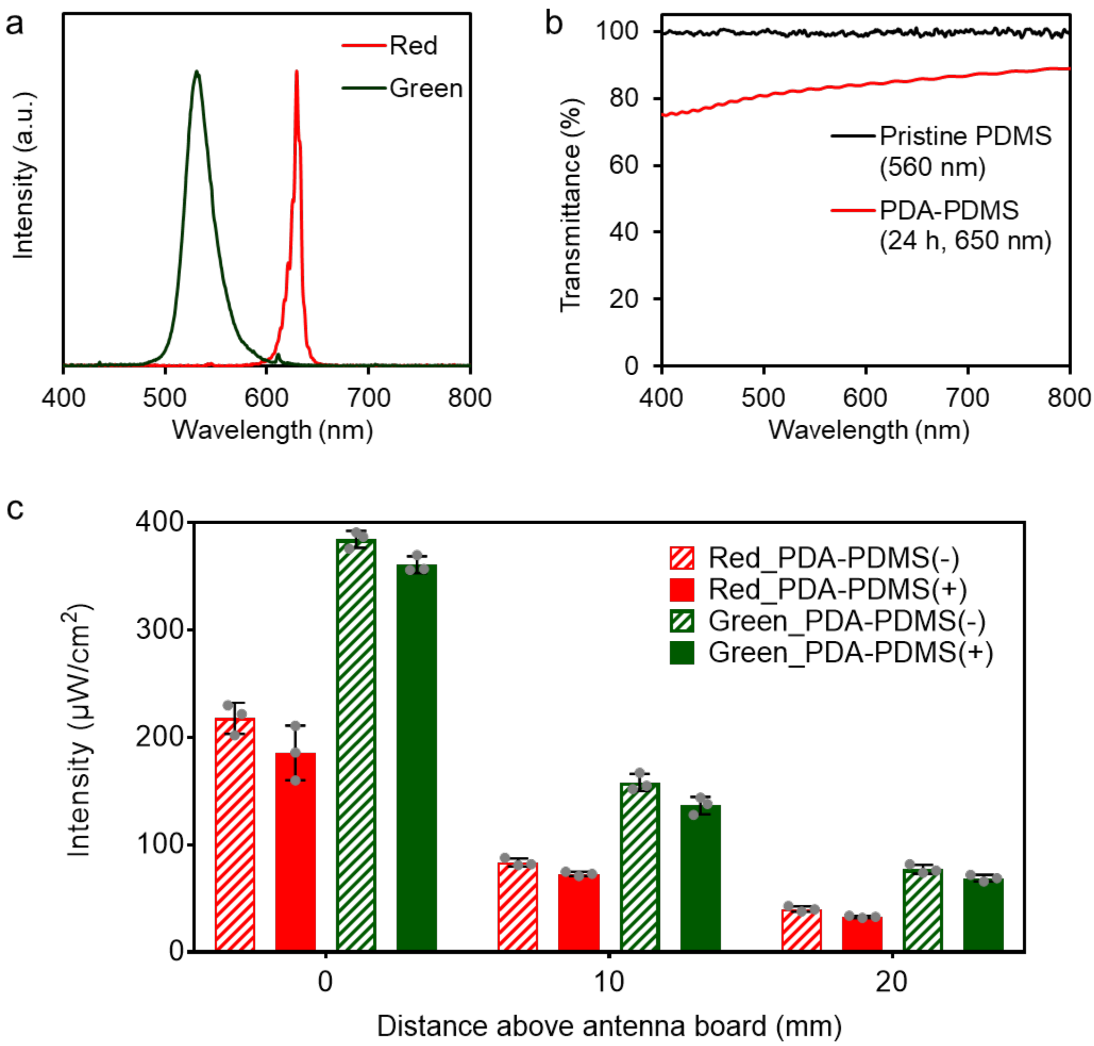

Supplementary Fig. 10 | Optical characterization of LED chips and PDA-PDMS nanosheets. a, Emission spectra of red and green LED devices. The measurement was repeated for three different LED chips for each color and a similar spectrum was obtained for every experiment. The representative spectra are shown. **b,** Transmittance spectra of pristine and PDA-PDMS nanosheets in the range of visible light. The measurement was repeated for three different samples for each nanosheet and a similar spectrum was obtained for every experiment. The representative spectra are shown. **c,** Relationship between distance above the antenna board and light intensity of red and green LED chips with/without (+/−) covering by PDA-PDMS nanosheet (650 nm). The error bars and the measures of centre represent the s.d. and the mean, respectively (n = 3 for each sample). Each data point is overlaid on the bars as gray dot plots.

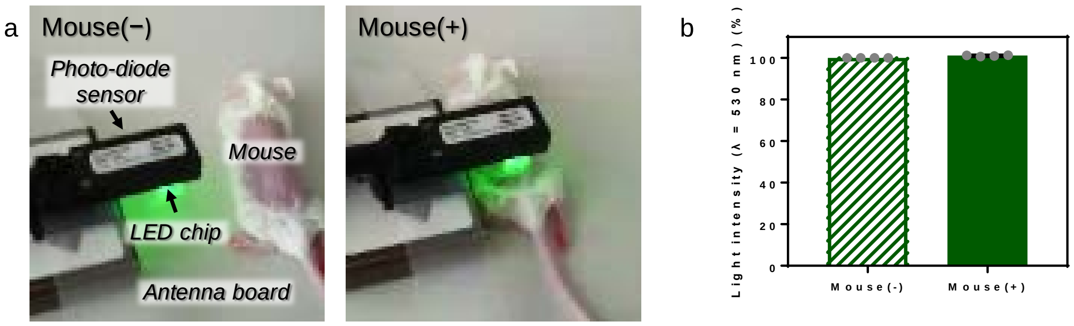

Supplementary Fig. 11 | Evaluation of influence of animal body on wireless power feeding between antenna board and LED chip. a, Images of the experimental setup for measurement of the light intensity of the LED chip (green) when a mouse is placed between the antenna board and the device or not. Left: Mouse(−) and right: Mouse(+). **b,** The change in the light intensity of the green LED chip (λ = 530 nm) between without (−) and with (+) a mouse between the antenna board and the device. The error bars and the measures of centre represent the s.d. and the mean, respectively (n = 4 different mice). Each data point is overlaid on the bars as gray dot plots.

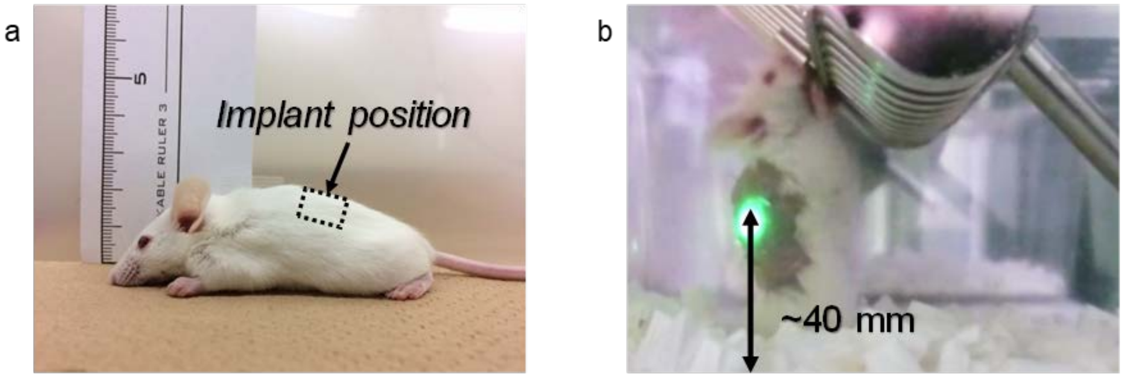

Supplementary Fig. 12 | Images of mouse for estimating the distance between implanted device and antenna board. a, Image of a mouse lying down with the belly on the floor; the distance between the implant position and the antenna board (floor) is ca. 20 mm. **b,** Image of a mouse standing up to take the bait from the ceiling; the distance between the implanted device and the antenna board was ca. 40 mm.

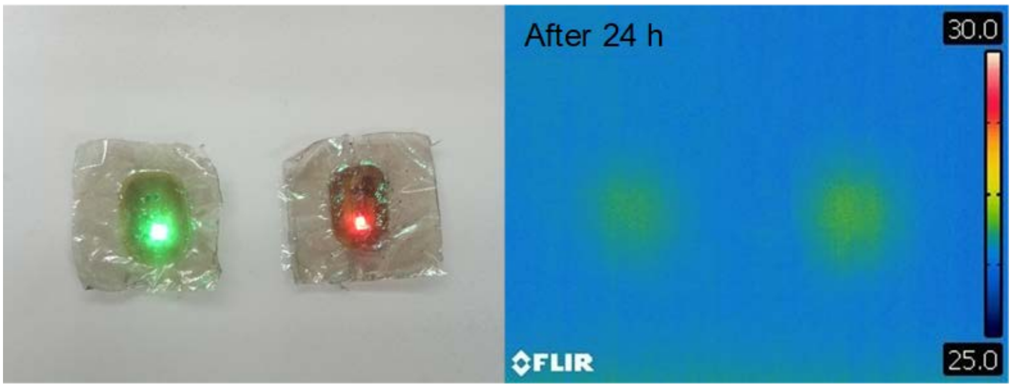

Supplementary Fig. 13 | Temperature increase of implants. Digital (left) and thermograph (right) image of green and red LED devices on an antenna board after 24 h of wireless powering.

Legends for Supplementary Videos 1-7:

Supplementary Video 1 | LED emission in two mice, each of which was implanted with a NFC-based red or green LED device. *ON*: the reader–writer is turned on. *OFF*: the reader–writer is turned off.

Supplementary Video 2 | A mouse with a pair of red LED devices implanted under the dorsal skin is moving vigorously in a cage.

Supplementary Video 3 | A mouse with a pair of green LED devices implanted under the dorsal skin is moving vigorously in a cage.

Supplementary Video 4 | Experimental set-up for a tack test to evaluate the adhesive energy between PDMS and chicken muscle. The PDMS supported by a square frame made of poly(vinyl chloride) (PVC) was attached to the surface of chicken muscle. The square frame was lifted up with a tensile tester until the PDMS was completely detached.

Supplementary Video 5 | Intradermal injection of cancer cells (Colon-26) in the dorsal skin of a mouse.

Supplementary Video 6 | Implanted LED device on the inner surface of the dorsal skin (opened skin) does not move even when the skin is stretched, compressed, and twisted.

Supplementary Video 7 | Implanted LED device on the inner surface of the dorsal

skin (closed skin) does not move even when the skin is stretched, compressed, and twisted.